

Predictors of cavitation in glassy polymers under tensile strain: a coarse grained molecular dynamics investigation

Ali Makke^{a,b}, Michel Perez^b, Jörg Rottler^c, Olivier Lamé^b, Jean-Louis Barrat^a

^a*Université de Lyon- Univ. Lyon I - LPMCN - UMR CNRS 5586- F69622 Villeurbanne, France*

^b*Université de Lyon - INSA Lyon - MATEIS - UMR CNRS 5510 - F69621 Villeurbanne, France*

^c*Department of Physics and Astronomy, University of British Columbia, 6224 Agricultural Road, Vancouver, BC, V6T 1Z1, Canada*

Abstract

The nucleation of cavities in a homogenous polymer under tensile strain is investigated in a coarse-grained molecular dynamics simulation. In order to establish a causal relation between local microstructure and the onset of cavitation, a detailed analysis of some local properties is presented. In contrast to common assumptions, the nucleation of a cavity is neither correlated to a local loss of density nor, to the stress at the atomic scale and nor to the chain ends density in the undeformed state. Instead, a cavity in glassy polymers nucleates in regions that display a low bulk elastic modulus. This criterion allows one to predict the cavity position before the cavitation occurs. Even if the localization of a cavity is not directly predictable from the initial configuration, the elastically weak zones identified in the initial state emerge as favorite spots for cavity formation.

Email address: `ali.makke@insa-lyon.fr` (Ali Makke)

Keywords: Cavitation, Plasticity, Computational modeling, Molecular dynamics simulation, Mechanical properties.

1. Introduction

Under hydrostatic stress conditions, failure of amorphous polymers occurs through cavitation, often followed by crazing, *i.e.* the formation of interpenetrating micro-voids [1]. Similarly, the plastic deformation of semi-crystalline polymers is strongly correlated to the nucleation of cavities in the amorphous region [2]. Although essential to control deformation and failure of many organic materials, cavitation in glassy polymers under load is poorly understood. To our knowledge, the microstructural causes, or the precursors of cavitation at a microscopic scale, are not clearly identified. Although it is known that impurities or surface defects aid the nucleation of cavities [3, 4], it is presently not possible to predict where cavitation will take place in the polymer.

Classical nucleation theory, where elastic energy is balanced by the creation of free surface, was used by Argon to model the cavitation nucleation [4]. Estevez *et al.* investigated the fracture toughness in glassy polymers using mechanical approaches with empirical constitutive equations to describe the competition between shear yielding and crazing [5]. They noted that the development of crazes is favored by a fast local deformation.

According to Gent [6], crazing in glassy plastics can be attributed to a local stress-activated devitrification. It is generally agreed that large triaxial tensile stresses are needed to induce cavitation, which forms the basis of several macroscopic craze initiation and cavitation criteria [7, 8]. Molec-

23 ular dynamics simulations of polymer glasses also found a transition from
 24 shear yielding, which obeys a pressure-modified von Mises yield criterion [9],
 25 to cavitation as the hydrostatic pressure becomes negative, but have not
 26 yet investigated the connection between cavitation and local microstructural
 27 configuration. More recent simulations explored correlations between the lo-
 28 cation of failure, higher mobility regions and a higher chain ends density [10]
 29 acting then as local defects, or a local, stress-induced disentanglement of
 30 chains [11]. In the latter work a primitive path algorithm was used to mon-
 31 itor the entanglement network in a sample undergoing triaxial deformation,
 32 and it was found that regions undergoing crazing were also depleted in terms
 33 of entanglements.

34 The local mechanical properties are a determining factor to understand
 35 the response of systems under strain. Yoshimoto et al. [12, 13] have cal-
 36 culated the local elastic modulus in a coarse grained polymer glass using
 37 a thermodynamic approach based on stress fluctuation . They found that
 38 polymers are mechanically heterogenous at local scale. Papakostantopoulos
 39 et al. [14] have studied the earliest local plastic events observed in the elastic
 40 regime of polymer glass. They found that these irreversible events take place
 41 in domains that exhibit a low positive elastic modulus. Analogous results
 42 were obtained by Tsamados et al. on Lennard-Jones glasses submitted to a
 43 quasistatic shear strain[15]. They found a correlation between high nonaffine
 44 displacements and local low elastic modulus.

45 It is unclear, however, if these criteria can be used in a predictive manner,
 46 in the sense that the cavitation event could be predicted from the configura-
 47 tion of an unstrained system.

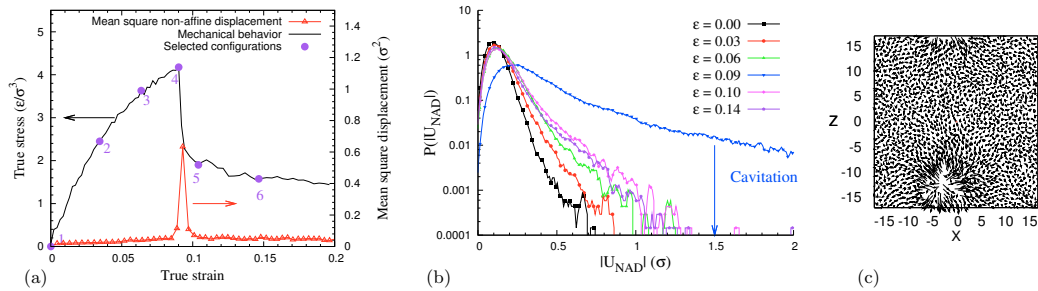


Figure 1: (a) Stress-strain curve of a glassy polymer at $T = 0.2$ during a triaxial tensile test. A peak in the mean square non-affine displacement is observed simultaneously with the drop of the stress due to cavitation. Markers 1, 2, 3 and 4 indicate the selected configurations for which distributions of NAD are plotted in (b). These distributions show an exponential tail for configuration 4, due to the large amplitude motions caused by cavitation. (c) Representation of the NAD in a cross-section of the sample containing the cavity, for configuration 4.

48 In this paper, we will therefore investigate the correlation between the
49 microstructure of a homopolymer at the segmental level and the nucleation
50 of cavities, in an attempt to find a microstructural *predictor* of such events.
51 Section 2 will present the methodology and will demonstrate that the non-
52 affine particle displacement (NAD) is a particularly suitable tool for charac-
53 terizing and locating cavities. Section 3 will be devoted to the investigation
54 of possible causes of cavitation, namely (i) local excess of free volume, (ii)
55 local excess of atomic stress, (iii) local density of beads and chain ends, and
56 (iv) local bulk modulus. We will show that while (i)-(iii) bear little correla-
57 tion to the NAD, the local bulk modulus (iv) has a much better potential to
58 predict the cavitation event.

2. Methods

2.1. Molecular dynamics simulations

Molecular dynamics (MD) simulations were carried out for a well established coarse-grained model, in which the polymer is treated as a linear chain of N beads of mass m , which we refer to as monomers, connected by stiff anharmonic springs that prevent chain crossing and breaking [16]. The beads interact through a conventional 6-12 Lennard-Jones potential that is truncated at 2.5 times the particle diameter (The tiny discontinuity of the force at the cutoff distance, less than 1% of the maximal attractive part, has no consequence). All quantities will be reported in units of the Lennard-Jones length scale σ and energy scale ϵ , and the characteristic time is $\tau_{LJ} = \sqrt{m\sigma^2/\epsilon}$. Newton’s equations of motion are integrated with the velocity Verlet method and a time step $\Delta t = 0.006$. Periodic simulation cells of initial size $L_x(0) = L_y(0) = L_z(0) = 34.2$ containing $M = 215$ chains of size $N = 200$ beads were used with a Nosé-Hoover thermostat, *i.e.* in the NVT ensemble. All samples were generated using the “radical-like” polymerization method [17]. The polymerization starts from a Lennard-Jones liquid, where 215 beads are chosen randomly to behave as “radical” sites. Each radical bead is allowed to connect to a free and nearest neighbor with a strong covalent bond. The radical sites are then transferred to the new connected beads, allowing thus the growth of all chains. If no monomers are near the radical, no FENE bond is created. Another attempt will be performed at the next growth stage. Between two growth stages, the entire system is relaxed during 100 MD steps. The polymerization propagates until all chains reach their target length of 200 beads. When the generation is terminated, residual

84 single beads are removed and the system is relaxed for 10^7 MD steps in NPT
 85 ensemble at $T = 1$ and $P = 0$ to reach an equilibrium state. The equilibra-
 86 tion leads to a “mean square internal distance” very close to the function
 87 given by Auhl et al. [18]. The polymer is then rapidly quenched into the
 88 glassy state at a temperature $T = 0.2$ in NPT ensemble (cooling rate: 1ϵ
 89 per 10^6 MD steps). The glass transition temperature is $T_g = 0.43$ ¹. The
 90 pressure remains zero and the sample density reaches 1.04 before applying
 91 the deformation.

92 Triaxial tensile test conditions were employed [19]. The samples were
 93 subjected to a sequence of deformation-relaxation steps, composed of (i) a
 94 rescaling of the simulation box in the tensile direction (y in our case so that
 95 the true strain $\epsilon_{yy}(t) = \ln(L_y(t)/L_y(0))$, whereas the two other dimensions
 96 remain unchanged, followed by (ii) an MD step in the NVT ensemble. The
 97 deformation rate was chosen to be $\dot{L}_y = 0.0025$, so that the initial strain
 98 rate is $\dot{\epsilon}_{yy}(0) = 7.3 \times 10^{-5}$. Over the range of strain investigated, the true
 99 strain rate remains essentially constant. Note that the applied deformation
 100 trajectory leads to a high level of triaxiality, which is the basic ingredient for
 101 cavitation. As the deformation proceeds, configurations were recorded along
 102 the trajectory in order to analyze their microstructure.

¹ T_g has been determined by the slope change observed when the sample volume is
 plotted with respect to the temperature during cooling from $T = 1$ to $T = 0.0001$ under
 the NPT ensemble

103 2.2. *Non-affine displacement: a tool for characterizing cavitation*

104 The mechanical behavior of our glassy polymers under triaxial tensile
105 conditions is illustrated in Figure 1(a). Three main regimes can be distin-
106 guished: (i) elastic, (ii) viscoelastic, and (ii) drawing regime, which occurs
107 at constant stress. In the elastic regime, the increase of deformation will
108 slightly shift the bead positions from their local energy minima, resulting
109 in reversible behavior. This regime is limited to a very low strain 0.001 as
110 demonstrated by Schnell [20]. In the viscoelastic regime, stress is relaxed by
111 inter-chain sliding. This stage is limited by a strong drop of stress. When
112 a critical deformation is reached, cavities will nucleate and then part of the
113 stored elastic energy is released as free surfaces open up. Note that the strain
114 hardening regime is not shown in Figure 1(a), since it occurs at larger strains
115 when the entanglement network of chains and fibrils becomes stretched [9].

116 The detection of cavity nucleation could be performed visually on snap-
117 shots that are regularly stored during the course of the tensile test. How-
118 ever, small cavities in a three dimensional sample can be delicate to observe.
119 Therefore, a more versatile indicator is needed. The non-affine displacement
120 (NAD) is the perfect candidate for such observation and has been success-
121 fully used to monitor local plastic activity in 2D amorphous Lennard-Jones
122 packings under athermal quasistatic deformation [21]. Note that NAD fluc-
123 tuations can not find their origin in the thermal motion of atoms since, in
124 the framework of this paper, specimens are maintained well below their glass
125 transition temperature ($T = 0.2 < T_g = 0.43$). Moreover, the NAD can be
126 used as a routine tool and it starts to increase locally, in the early stages
127 of cavity nucleation, even before the cavity could be observed visually on a

128 snapshot of the sample.

129 The non-affine displacement (\mathbf{u}_{na}^i) is defined as the difference between
 130 the mean displacement of a bead i during time δt ($\mathbf{r}^i(t + \delta t) - \mathbf{r}^i(t)$), and
 131 the mean displacement it would experience if the deformation were perfectly
 132 affine, *i.e.* homogeneous at all scales,

$$\mathbf{u}_{na}^i(t) = \mathbf{r}^i(t + \delta t) - \mathbf{r}^i(t) - \dot{\epsilon}_{yy}(t)\delta t r_y^i(t)\mathbf{e}_y, \quad (1)$$

133 where $\mathbf{r}^i(t)$ is the position of bead i at time t , $r_y^i(t)$ is the projection of
 134 this position along along the y axis and δt is the time elapsed between two
 135 configurations where the NAD is evaluated (typically 30τ).

136 In Figure 1(a), the cavity nucleates at $\epsilon_{yy} = 0.09$. At the same strain,
 137 the NAD exhibits a peak. Beads that exhibit the largest NAD are those
 138 which belong to the surface of the cavity (see Figure 1(c)). Figure 1(b)
 139 shows the evolution of the NAD distribution for several deformations. Before
 140 cavitation, increasing the deformation shifts the distribution tail to larger
 141 NAD until the very moment at which the growth of a cavity occurs, which is
 142 associated with very large values of NAD (see Figure 1(c)). A threshold for
 143 NAD magnitude has been defined: if $|\mathbf{u}_{na}^i| > 1.5\sigma$ at the yielding point, the
 144 bead i is said to belong to the cavity surface. This threshold is used to identify
 145 the “cavity beads” in order to follow some of their local properties. The
 146 position of the cavity is defined as the centre of mass of these “cavity beads”.
 147 After cavitation, the distribution returns to a narrower shape. Note that the
 148 NAD distribution broadens even before the stress drop in the stress-strain
 149 curve, due to the nucleation of the cavity. In the following sections, NAD
 150 will be used as a quantitative tool for investigating the possible correlations
 151 with other microstructural or mechanical properties, such as Voronoi volume,

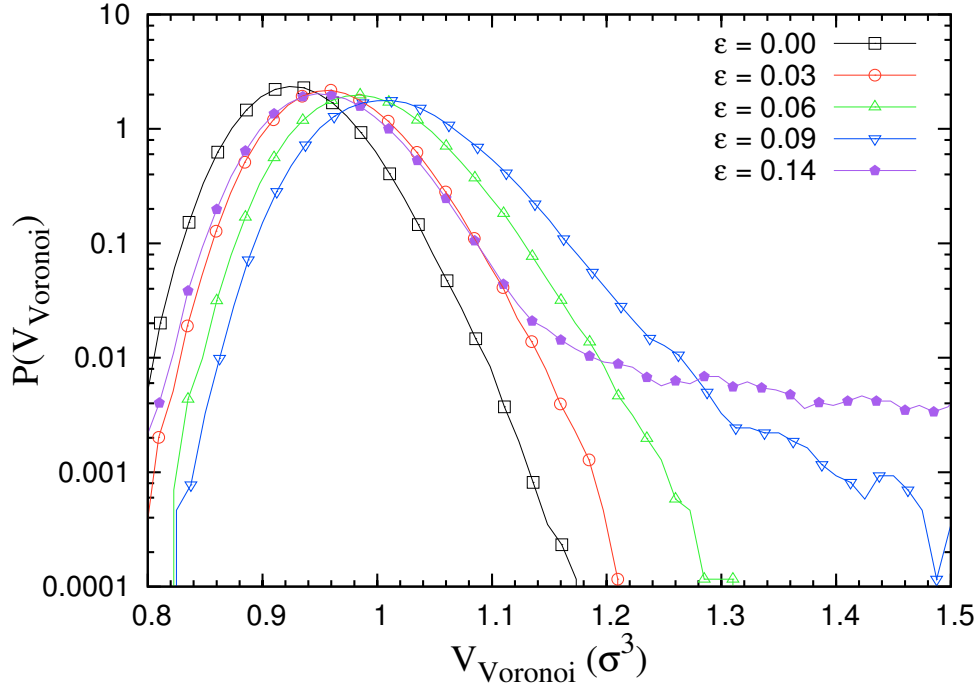


Figure 2: Voronoi volume distributions of configurations extracted over the deformation trajectory. Cavitation can be clearly seen in the tail of distribution. After cavitation, the distribution reverts to a narrower shape.

152 hydrostatic stress, local density and local moduli.

153 3. Microstructural causes and precursors of cavitation

154 In this section, we will attempt to correlate NAD fluctuations with some
 155 local properties measured at the scale of a single “atom” (Voronoi volume
 156 and stress per atom), and properties averaged on the scale of a few particle
 157 diameters (chain end density and bulk modulus).

158 *3.1. Voronoi volume fluctuations*

159 The concept of free volume has been extensively used to explain many
160 specific properties of supercooled liquids and glasses. Free volume is defined
161 as the volume in excess compared to an ideal disordered atomic configuration
162 of maximum density. One of the simplest way to compute free volume on a
163 local scale (and to avoid the ambiguity of the above definition) is the Voronoi
164 tessellation, which uniquely assigns a polygonal volume to each bead, formed
165 by intersecting the planes bisecting the lines between different bead centres.
166 In order to determine whether local fluctuations of free volume (or Voronoi
167 volume) favour the nucleation of a cavity, we used the voro++ routine to
168 calculate the volume associated to each bead ².

169 *Voronoi volume and deformation level..* Figure 2 shows the effect of the de-
170 formation on the Voronoi volume distribution. Increasing the deformation
171 will increase almost homogeneously the free volume until cavitation takes
172 place. During and after cavitation, the Voronoi volume distribution exhibits
173 a significant tail representing the beads belonging to cavity walls. Note that
174 after cavitation, the distribution relaxes to a narrower shape. Therefore, the
175 cavitation process can be seen as an event, which *localizes* or *precipitates* the
176 excess of free volume introduced by deformation.

177 *Voronoi volume and beads functionality..* Figure 3 compares the mean Voronoi
178 volume evolution of both regular beads and chain ends. It can be seen that
179 chain ends exhibit a larger Voronoi volume, which is not surprising since, by

²See <http://math.lbl.gov/voro++/> and ref. [22], where a very early version of this code was used.

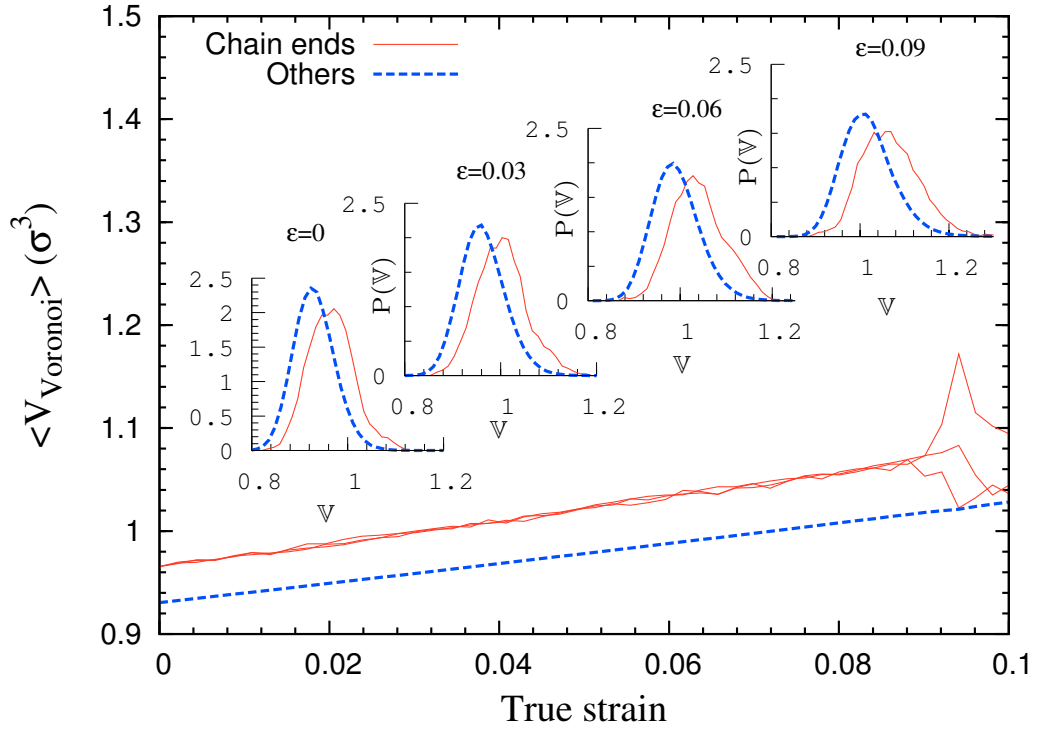


Figure 3: Evolution of the mean Voronoi volume of chain ends and other beads. Inset: Voronoi volume distributions during the course of deformation. No correlation can be observed between chain ends and Voronoi volume variation during tensile test.

180 construction, covalent and Lennard-Jones bonds have their energy minimum
 181 at 0.9σ and 1.12σ , respectively. Note that when cavitation occurs, the mean
 182 Voronoi volume of chain ends becomes very noisy due to statistical limita-
 183 tions. The insets of Figure 3 show that the Voronoi volume distributions
 184 have a Gaussian shape, which shows the presence of low Voronoi volumes
 185 (much lower than the volume of an ideal disordered configuration). This
 186 calls into question the very concept of free volume, which is defined as that
 187 part of the atomic volume that can be redistributed throughout the system
 188 without change in energy [24, 25], *i.e.* the volume of an ideal disordered
 189 configuration. These points of extremely low volume could be related to the
 190 *constriction points* introduced by Stachurski [23] and, to a larger extent, to
 191 the *quasi-point defects* of Perez [1], which represent points of high fluctuation
 192 of free energy.

193 *Voronoi volume and non-affine displacement..* Within the free volume ap-
 194 proach, deformation induced relaxations are supposed to be correlated with
 195 the available free volume. Zones of larger free volume will therefore deform,
 196 changing the potential energy landscape and providing more free volume to
 197 zones of initially larger free volume. This explanation is often proposed to
 198 describe the formation of mechanical instabilities such as cavitation or shear
 199 bands. Motivated by these ideas, the search for a relationship between the
 200 magnitude of the NAD and the Voronoi volume becomes relevant.

201 Figure 4 shows a scatter plot obtained during deformation, where the
 202 magnitude of the NAD and the Voronoi volume were taken as variables. This
 203 scatter plot does not show a clear tendency for a correlation between NAD
 204 and Voronoi volume. Free volume represents the potential space for motion

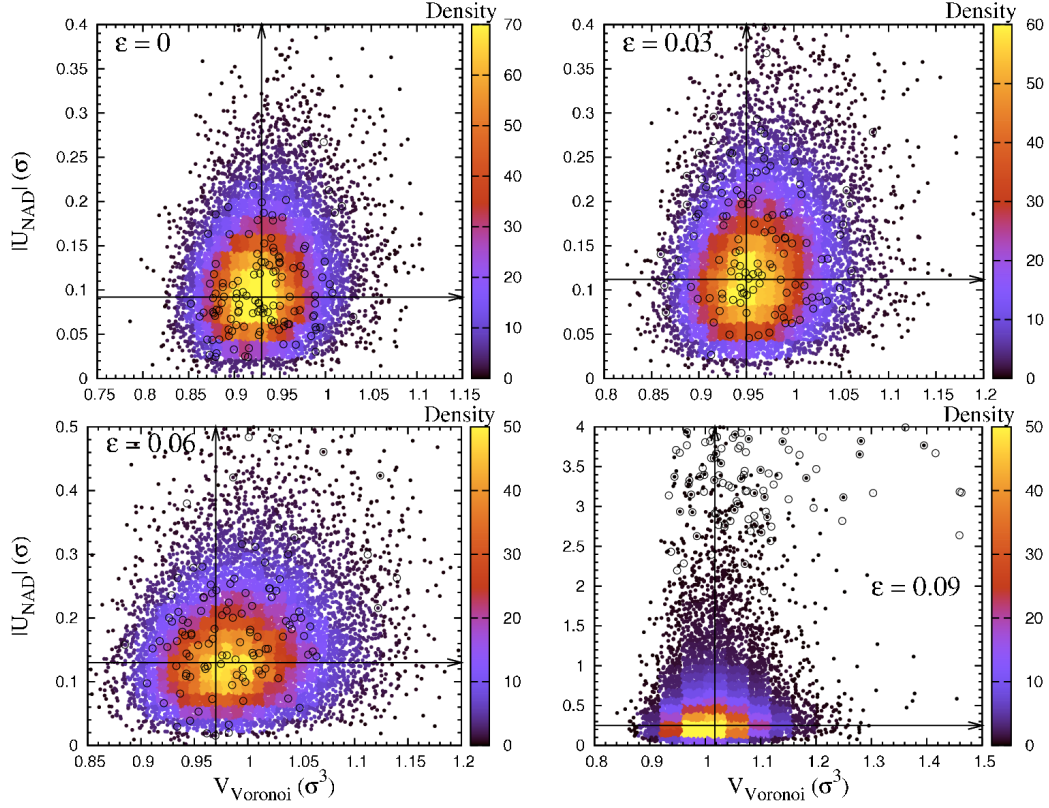


Figure 4: (Color online) NAD magnitude of beads plotted against their Voronoi volume at several strains $\epsilon=0, 0.03, 0.06$ and 0.09 (cavitation). Arrows describe the higher density value of each variable. No correlation was found between these variables for all strains. “Cavity cluster beads” are marked by the symbol \circ : no remarkable trend can be distinguished, except during cavitation, where they exhibit larger NAD and slightly larger Voronoi volume.

205 but it can not be seen as being a causal factor of the NAD and cavitation. The
 206 “cavity cluster” beads are also shown in this plot. In both cases, the points
 207 are distributed randomly and no noticeable trend was found, except during
 208 cavitation, where these beads exhibit larger NAD and slightly larger Voronoi
 209 volume. This analysis (not shown in this paper) was performed for several
 210 other temperatures ($T = 0.01$ and $T = 0.1$) and no correlation was found
 211 under these conditions either. Note that before cavitation, the magnitude of
 212 NAD remains much less than inter-atomic distance (σ), in other words, the
 213 deformation is purely affine.

214 3.2. Stress fluctuations

215 The local stress on any given bead can be obtained by dividing the classi-
 216 cal expression of the virial stress by the Voronoi volume \mathbb{V}_m of atom m [26],

$$217 \sigma_{ij}^m = -\frac{1}{2\mathbb{V}_m} \left(m_m v_i^m v_j^m + \sum_{n \neq m} r_i^{mn} \cdot f_j^{mn} \right), \quad (2)$$

218 where v_i^m is the velocity i th component of atom m ; f_i^{mn} and r_i^{mn} are
 219 the i th component of force and distance between two interacting atoms m
 220 and n , respectively. The first term of this equation represent the kinetic
 221 contribution and the second one is the Cauchy stress. The hydrostatic stress
 222 S_{hyd} was calculated by computing the trace of the stress tensor, $S_{hyd} =$
 223 $-(\sigma_{11} + \sigma_{22} + \sigma_{33})/3$

224 Figure 5 compares the distributions of hydrostatic stresses at several
 225 strains during deformation. In the initial undeformed configuration, the dis-
 226 tribution shows an exponential tail towards negative values. As the deforma-
 227 tion increases, the negative values of the hydrostatic stress are progressively

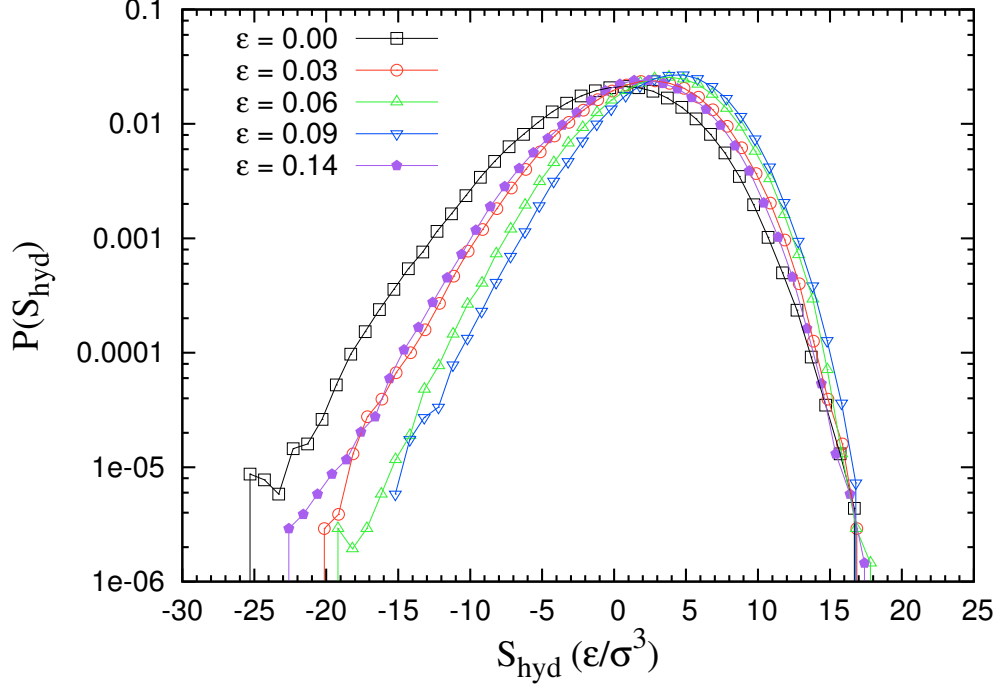


Figure 5: Distribution of hydrostatic stress at different deformation levels. The distribution narrows until the cavity opens, then broadens again.

228 relaxed, so that the distribution narrows and becomes more symmetrical
 229 just before cavitation takes place. These results are consistent with those
 230 of ref [26]. After the cavitation has occurred, large negative values of the
 231 stress are again obtained, since the average free space is decreased as shown
 232 previously in Figure 2.

233 In order to investigate the correlation between NAD and the atomic hy-
 234 drostatic stress, a scatter plot of these quantities is displayed in Figure 6.
 235 Apparently, there is no direct trend for a correlation between NAD and the
 236 hydrostatic stress at the scale of individual beads. The hydrostatic stress was

237 also evaluated by considering each contribution separately (pair, bonded) at
 238 several strains, and again no correlations were found. When specific beads
 239 (chain ends and cavity cluster) values are selected in these scatter plots, the
 240 corresponding points appear to be a randomly chosen subset of the total
 241 sample. This absence of correlation may appear surprising, as the presence
 242 of a high local stress is often expected to result in plastic deformation. Note
 243 however that this result is consistent with a recent study [26] which showed
 244 no correlation between atomic stresses and shear yielding in polymers. In
 245 an analogous way, a previous study on sheared glasses [27] also failed to
 246 find a direct correlation between local stresses and the relevant local plastic
 247 deformation (shear transformations in that case).

248 It may be, however, that a more coarse grained characterization is nec-
 249 essary to identify such correlations, and that the cavitation events are the
 250 result of a local heterogeneity that extends beyond the scale of individual
 251 beads. In order to assess this hypothesis, we describe briefly in the next
 252 section studies performed on density fields defined at a more coarse grained
 253 scale.

254 *3.3. Coarse grained densities*

255 The opening of a cavity under strain can be seen as a collective event, that
 256 involves at least those atoms that will form the cavity “skin” at the end of
 257 the process. The corresponding mechanical instability may therefore be the
 258 result of some density anomaly that extends over a region larger than a single
 259 atom size or Voronoi cell. We therefore have also explored the properties of
 260 our polymer system on such a coarse grained scale by defining continuous
 261 fields from the atomic positions. Various possibilities are available for such a

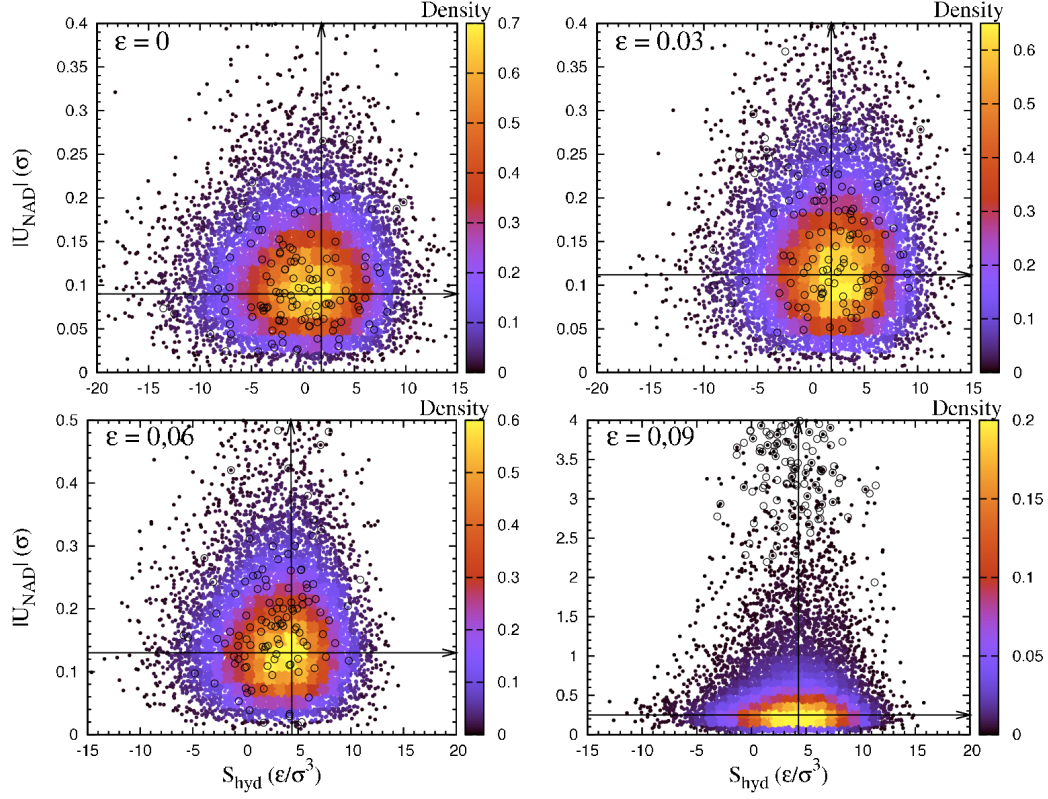


Figure 6: (Color online) Scatter plot of the non affine displacement against hydrostatic stress shown at the same deformation as in Figure 4. No clear trend for a correlation can be established. The values corresponding to the beads that surround the cavity labeled by the symbol \circ are randomly dispersed, thus preventing one to identify any specific correlation for these beads.

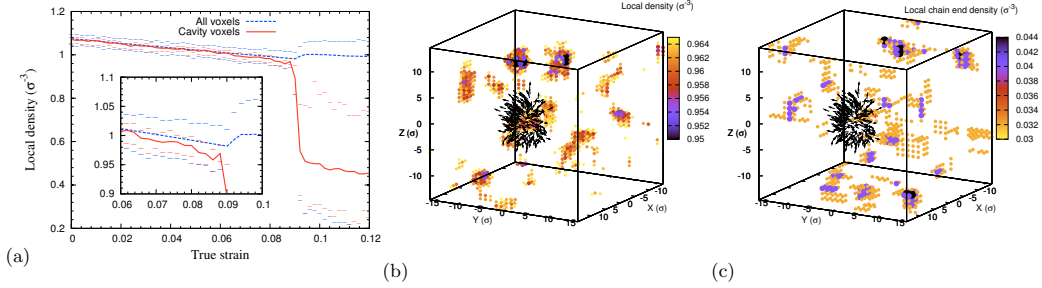


Figure 7: (Color online) Evolution of mean local density calculated within cubic bins of size $5 \times 5 \times 5 \sigma^3$. The average of the overall voxels (dashed line) is compared with the average of voxels that are associated with the cavity cluster beads (solid line). Symbols (-) denote the upper and lower values for each curve. The spatial distribution of local density taken at $\epsilon = 0.08$ is shown in (b) and the corresponding map of chain end density in (c). The arrows describe the non affine displacement of the “cavity cluster beads”. The dark spots identify the low density vicinities (b) and the high chain end density (c).

coarse graining procedure [28, 15, 29]; here we choose the simplest one, which consists in computing the densities on a regular grid by assigning to each grid node the atoms that belong to a fixed “voxel” volume around this node. The voxel size is taken in the range 5σ to 7σ , which was shown in similar studies [30, 26, 14] to permit a good description in terms of continuous fields (with about 120 monomers per voxel) while preserving the locality and possible spatial heterogeneity of the variables under consideration.

We have attempted to coarse grain and to correlate with the appearance of cavities two of the densities examined previously at the atomic level, namely the density of chain ends and the density of monomers. The local density field is defined as:

$$\rho_i = \frac{n_i}{\sum_j \mathbb{V}_i^j} \quad (3)$$

where n_i is the number of beads within a voxel i , and \mathbb{V}_i^j is the Voronoi

274 volume of the bead j that is included in the voxel i . Figure 7(a) shows the
275 evolution of this local density with strain, and compares the average value
276 with the value observed in the vicinity of the cavity.

277 These data show that the local density in the vicinity of the cavity fol-
278 lows the mean value until a deformation of $\epsilon = 0.06$. Although cavitation
279 does not occur until $\epsilon = 0.09$, the local volume begins to decrease earlier
280 (see inset). This observed trend can be interpreted by the fact that cavi-
281 tation starts earlier than the drop of stress in the stress-strain-curve. This
282 “pre-cavitation” behavior can be interpreted as resulting from a dynamical
283 equilibrium between the elastic energy and the free surface energy of cavity
284 with relatively small radius. This situation remains stable until the cavity
285 reaches a critical radius (roughly estimated 2σ), beyond which the size of
286 the cavity increases rapidly. The spatial distribution of the local density at
287 $\epsilon = 0.08$, just before the opening the cavity is shown in part (b) of Figure
288 7. The lowest density spots are far from the expected position of the cavity,
289 but a low density can be noticed in the cavity vicinity. In general, we have
290 checked that a systematic decrease in density prior to cavitation is specific of
291 the points that are located in the vicinity of the emerging cavity. Other points
292 may display fluctuations in their values of the density, but these fluctuations
293 remain uncorrelated with cavitation events. After the cavity nucleation, the
294 low density regions that did not form cavities release their excess free volume
295 introduced by the triaxial deformation condition. Therefore the local density
296 of such regions return to values similar to regions that are not involved in
297 the cavitation. In conclusion, local loss of density should be seen rather as a
298 consequence than as a cause of cavity nucleation.

299 As was mentioned above (in section 3.1), the free volume was found to be
 300 correlated with the bead connectivity. Chain ends exhibit a higher Voronoi
 301 volume compared to other monomers, and a lower density of beads could be
 302 expected where a higher density of chain ends is present. We therefore define
 303 a local density of chain ends $\rho^{C.E.}$ as

$$\rho_i^{C.E.} = \frac{n_i^{C.E.}}{V_i}, \quad (4)$$

304 where $n_i^{C.E.}$ is the number of chain ends within a voxel i , and V_i is the volume
 305 of the voxel. Figure 7(c) shows that, at this level of coarse graining, the spa-
 306 tial distribution of chain ends is uncorrelated with the local density of beads
 307 and also with the cavity position. This indicates that the modification of the
 308 packing density by the presence chain ends is insignificant. Summarizing, the
 309 coarse grained density of beads exhibits a limited success as a predictor for
 310 cavity formation, as its evolution can be correlated with the formation of a
 311 cavity only shortly before the event actually takes place. The coarse grained
 312 density of chain ends, on the other hand, does not correlate well with the
 313 total density or with cavitation.

314 3.4. *Local mechanical properties*

315 Our last attempt to identify a microstructural predictor for cavitation
 316 events is inspired by previous work on simple glassy systems under shear
 317 deformation, in which a low value of the shear moduli was identified as a
 318 good indicator for the occurrence of the relevant local plastic events, shear
 319 transformation zones [15, 14]. Here the relevant events involve a local dilata-
 320 tion of the material which eventually gives rise to a cavity, and points to the
 321 local bulk modulus as a possible predictor.

Local heterogeneity in the elastic properties of glasses is now a well documented feature, with a number of studies having shown that the moduli defined at intermediate scales (of the order of 10 atomic sizes) are those of an isotropic but heterogeneous material. At such scales, a typical glassy sample can be described as consisting of coexisting “hard” and “soft” regions. This behavior is independent of the precise method which is used to define the coarse grained elastic constant, which may involve either the use of statistical mechanical formulae at a local scale [13, 14], or exploiting the linear relationship between coarse grained stress and strain field [15]. Here we present results for the local bulk modulus obtained from a third approach, originally introduced by P. Sollich *et. al.* [31], which has the advantage of being easily implemented at a reduced computational cost. The method can be summarized as follows: one first defines a coarse graining volume as a fictive shape that encapsulates a number of beads. The shape was chosen spherical in order to reduce any potential boundary effects, and the radius equal to 3.5 particle diameters, consistent with the typical coarse graining scales used in other methods [15, 14]. The entire sample is then deformed affinely (in this case using a uniform dilation of all bead coordinates). After this homogeneous deformation, all beads are kept frozen, except those contained in the coarse graining volume which are allowed to fluctuate in a constant volume, constant temperature molecular dynamics trajectory (here we perform a trajectory at a rather low temperature, $T = 0.01$). The increase in the hydrostatic stress S_{hyd}^m within the spherical volume m is obtained from the virial stress formula, and the local modulus K^m can be defined by dividing

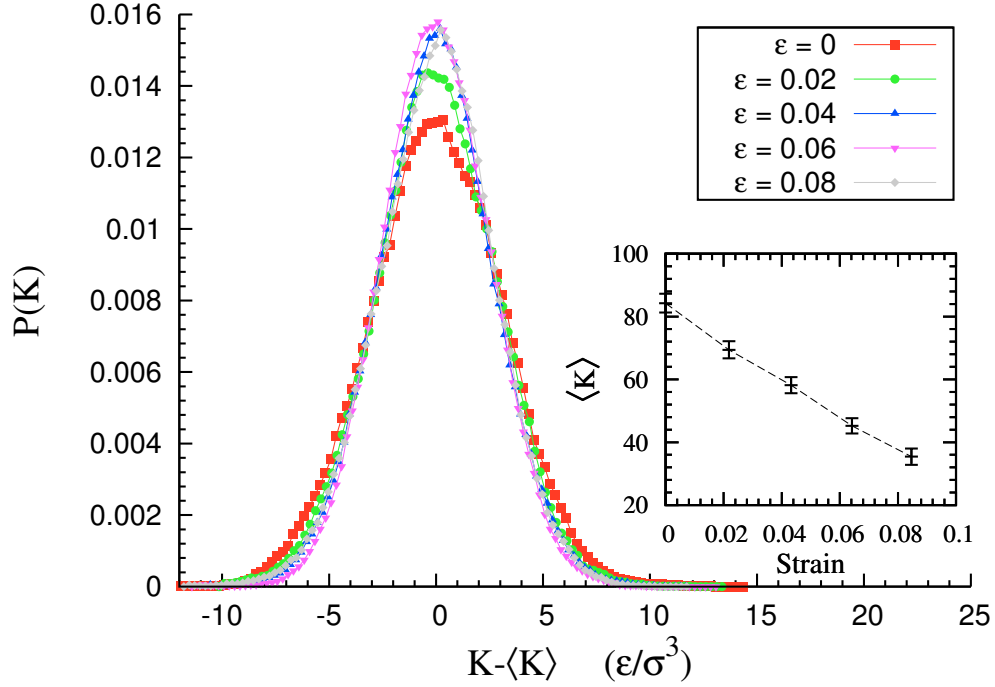


Figure 8: Density distribution of local bulk modulus for the same specimen at several deformation levels. Distributions are shifted by their mean values. The inset shows the evolution of the mean values. Error bars are deduced from the standard deviation.

346 this stress by the imposed increase in volumetric strain ϑ^m :

$$K^m = \frac{d(S_{hyd}^m)}{\vartheta^m}. \quad (5)$$

347 In order to improve the accuracy on K^m , it has then been averaged over
 348 a dozen expansion tests within the domain $0 < \vartheta^m < 10^{-5}$. A sequence of
 349 deformation (isotropic expansion) and relaxation steps is applied over the
 350 sample, the gauge volume V^m and S_{hyd}^m are measured after each step. The
 351 expansion is limited to a very low deformation amount since the measurement
 352 is restricted in the elastic regime only. Substituting the ϑ^m by its definition

353 $\frac{dV^m}{V^m}$ leads to another form of equation (5):

$$K^m \cdot \frac{dV^m}{V^m} = d(S_{hyd}^m) \quad (6)$$

354 or equivalently

$$K^m \cdot \ln(V^m)|_0^t = S_{hyd}^m|_0^t, \quad (7)$$

355 where V^m and S_{hyd}^m are integrated along the deformation trajectory from 0
 356 to t . This method allows us to obtain an accurate determination of K^m
 357 in the linear regime by fitting the data obtained for $S_{hyd}^m = f(\ln(V^m))$. This
 358 procedure was applied along each tensile deformation trajectory, for positions
 359 of the center of the coarse graining volume distributed on a regular grid.

360 Figure 8 compares the statistical distributions of the local bulk modu-
 361 lus at different strain levels. The plotted distributions are shifted by their
 362 mean values to facilitate comparison of their shapes. Curves remain sym-
 363 metrical and Gaussian, whatever the applied strain before cavitation. As the
 364 deformation increases, the distribution will become slightly narrower. This
 365 behaviour is consistent with the trend described in the previous sections, that
 366 the polymeric system tends to homogenize its local stress under an applied
 367 deformation. The mean value of the local bulk modulus (see inset) decreases
 368 continuously as the deformation increases and more free volume is introduced
 369 in the system.

370 In order to investigate the spatial distribution of the local bulk modulus,
 371 two-dimensional slices in a plane perpendicular to the tensile direction were
 372 taken at the level at which the cavity is observed. Figure 9 shows a sequence
 373 of such bulk modulus cartographies that are captured along the deformation
 374 trajectory. Each slice corresponds to one of the blue markers on the stress

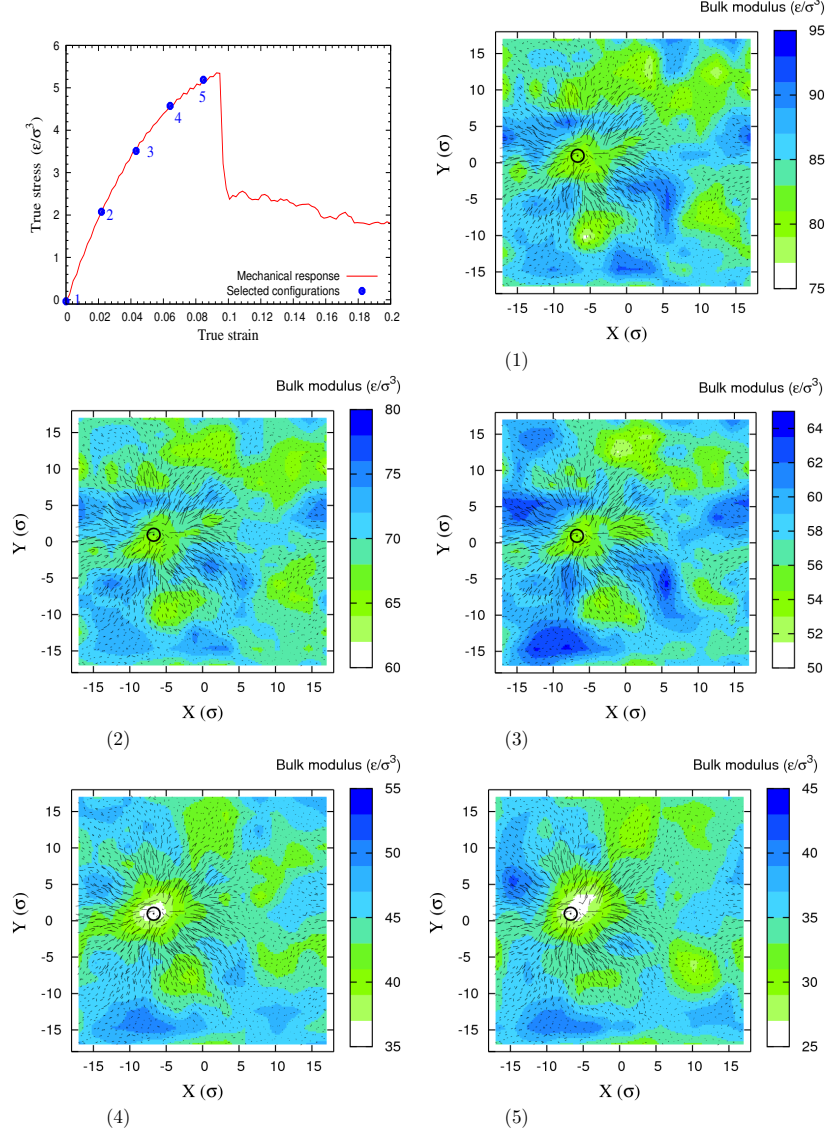


Figure 9: (Color online) XY Layers taken from the spatial distribution of the bulk modulus (tensile direction is Z in this case). The Z coordinate of all layers corresponds to the cavity position. Every layer is indexed (bottom left corner) referring to its position in the stress-strain curve on the upper left. These maps are superimposed with the nonaffine displacement at $\epsilon = 0.09$ that shows the formation of the cavity.

375 strain curve (first plot in figure 9). The nonaffine vectors describing the
 376 formation of a cavity are also plotted on each map. As can be seen, the local
 377 bulk modulus fluctuates between high and low values at each strain, and
 378 the position at which the cavity appears corresponds to one of the low bulk
 379 modulus sites identified in the starting configuration. When the deformation
 380 increases, an extremely low value of bulk modulus appears in the expected
 381 position of cavity, as in slices (4) and (5). The lower value indicated here is
 382 not only a local minimum in the plane of the figure, but instead corresponds
 383 to the lowest value for the entire sample.

384 In the light of this strong correlation between NAD and elastic modulus,
 385 the cavitation process in glassy polymers can be described in the following
 386 manner: The polymeric system exhibits some fluctuations in the local elastic
 387 bulk modulus. As the deformation progresses, the statistical distribution of
 388 the bulk modulus changes: The mean value decreases, but the contrast of
 389 spatial distribution is conserved. At relatively high strain, one of the zones
 390 that initially displayed a low bulk modulus will reach an anomalous value,
 391 resulting in a favorable location for the subsequent growth of a cavity.

392 We will now investigate whether this behavior should be described as
 393 deterministic (the cavity systematically forms in a particular zone) or rather
 394 statistical (the cavity forms randomly in one of the zones with a low modulus)
 395 process. To this end, the same system was subjected to three tensile tests
 396 with different tensile directions x , y and z . The positions at which cavitation
 397 takes place were recorded and compared after each test.

398 Figure 10(a) shows that, for the same initial configuration, cavities nu-
 399 cleate in different zones. The same behaviour was also found for several

400 systems with different temperatures. The cavities systematically nucleate in
401 zones that are characterized by a low modulus in the initial state, however
402 the specific site at which it is observed depends on the deformation path and
403 on the tensile direction.

404 4. Conclusions

405 In this work the relationship between a cavitation event in a glassy poly-
406 mer undergoing a tensile test and the local properties has been investigated
407 with molecular dynamics simulations. Several properties have been analyzed
408 at two different length scales: the elementary scale of the monomer, and a
409 coarse graining scale of 5 to 10 particle diameters. Independent of the scale
410 under consideration, we find that the density of monomers or the density of
411 chain ends do not correlate with the subsequent appearance of a cavity. In
412 contrast, the bulk modulus in the unstrained configuration displays fluctu-
413 ations that can be directly related, in a statistical sense, to the appearance
414 of a cavity at large deformations. Note that very similar conclusions were
415 reached by Toepperwein and de Pablo in a recent study that considered both
416 homopolymers and composite systems [32]. This situation resembles those
417 observed in glassy materials under volume conserving shear, where a weak
418 shear modulus indicates a tendency for plastic rearrangement.

419

420 **Acknowledgments:** Computational support was provided by the Feder-
421 ation Lyonnaise de Calcul Haute Performance and GENCI/CINES . The
422 financial support from ANR project Nanomeca is acknowledged. Part of
423 the simulations were carried out using the LAMMPS molecular dynamics

424 software (<http://lammmps.sandia.gov>).

References

- [1] J. Perez, *Physics and mechanics of amorphous polymers*, Balkema, Rotterdam (1998).
- [2] S. Humbert, O. Lame, J.M. Chenal, C. Rochas, G. Vigier *Macromolecules*, **43**, 7212-7221 (2010).
- [3] K. P. Herrmann and V. G. Oshmyan, *International Journal of Solids and Structures*, **39**, 3079-3104 (2002).
- [4] A. S. Argon and J. G. Hannoosh, *Phil. Mag.*, **36**, 1195-1216 (1977).
- [5] R. Estevez, M. G. A. Tijssens. and E. Van der Giessen *J. Mech. Phys. Sol.* **48** 2585-2617 (2000).
- [6] A. N. Gent, *J. Mater. Sci.*, **5**, 925 (1970).
- [7] S. S. Sternstein and L. Ongchin, *Polym. Prepr.*, **10**, 1117 (1969).
- [8] P. B. Bowden and R. J. Oxborough, *Phil. Mag.*, **28**, 547 (1973).
- [9] J. Rottler and M.O. Robbins, *Phys. Rev. E* **64**, 051801 (2001); *Phys. Rev. E* **68**, 011801 (2003).
- [10] B. Sixou *Molecular simulation* **33**, 965-973 (2007).
- [11] D. K. Mahajan, B. Singh, and S. Basu, *Phys. Rev. E*, **82**, 011803 (2010).
- [12] K. Yoshimoto, G.J. Papakonstantopoulos, P.F. Lutesko, J.J. de Pablo, *Phys. Rev. B* **71**, 184108 (2005).

- [13] K. Yoshimoto, T.S. Jain, K. Van Korkum, P.F. Nealey, J.J. de Pablo, *Phys. Rev. Lett.* **93** (2004).
- [14] G. J. Papakonstantopoulos, R. Riggleman, J.-L. Barrat, J. J. de Pablo, *Phys. Rev E* **77**, 041502 (2008).
- [15] M. Tsamados, A. Tanguy, C. Goldenberg, J.L. Barrat, *Phys. Rev. E* **80**,026112 (2009).
- [16] K. Kremer and G.S. Grest, *J. Chem. Phys.* **92**, 5057 (1990).
- [17] M. Perez, O. Lame, F. Leonforte and JL Barrat, *J. Chem. Phys.*, **128** 234904 (2008).
- [18] R. Auhl, R. Everaers, G. S. Grest, K. Kremer, and S. J. Plimpton, *J. Chem. Phys.*, **119**, 12718 (2003).
- [19] A. Makke, M. Perez, O. Lame, J.L. Barrat *J. Chem. Phys.* **131**, 014904 (2009).
- [20] B. Schnell, PhD. Université de Strasbourg (2006).
- [21] M. Tsamados, *Eur. Phys. J. E*, **32**, 165-181(2010).
- [22] C. H. Rycroft, G. S. Grest, J. W. Landry, M. Z. Bazant, *Phys. Rev. E* **74**, 021306 (2006).
- [23] Z. H. Stachurski, *Polymer* **44** 6067-6076 (2003).
- [24] D. Turnbull and M. Cohen, *J. Chem. Phys.* **34** 120 (1961).
- [25] D. Turnbull and M. Cohen, *J. Chem. Phys.* **52** 3038 (1970).

- [26] D. MacNeill, J. Rottler *Phys. Rev. E* **81**, 011804 (2010).
- [27] M. Tsamados, A. Tanguy, F. Leonforte and J.-L. Barrat *Eur. Phys. J. E*, **26**, 283-293 (2008).
- [28] I. Goldhirsch and C. Goldenberg *Eur. Phys. J. E*, **9**, 245-251 (2002).
- [29] F. A. Detcheverry, D. Q. Pike, P. F. Nealey, M. Muller, J. J. de Pablo *Faraday Discussions*, **144**, 111-125 (2010).
- [30] J.P. Wittmer, A. Tanguy, J.L. Barrat, L. Lewis *Europhys. lett.* **57** 423-429 (2002).
- [31] P. Sollich, A. Barra, “Through the mesoscopic looking glass: Exploring the rheology of soft glasses”, Preprint (2010).
- [32] G. N. Toepperwein, J.J. de Pablo, “Cavitation and Crazing in Rod-Containing Nanocomposites”, preprint 2011

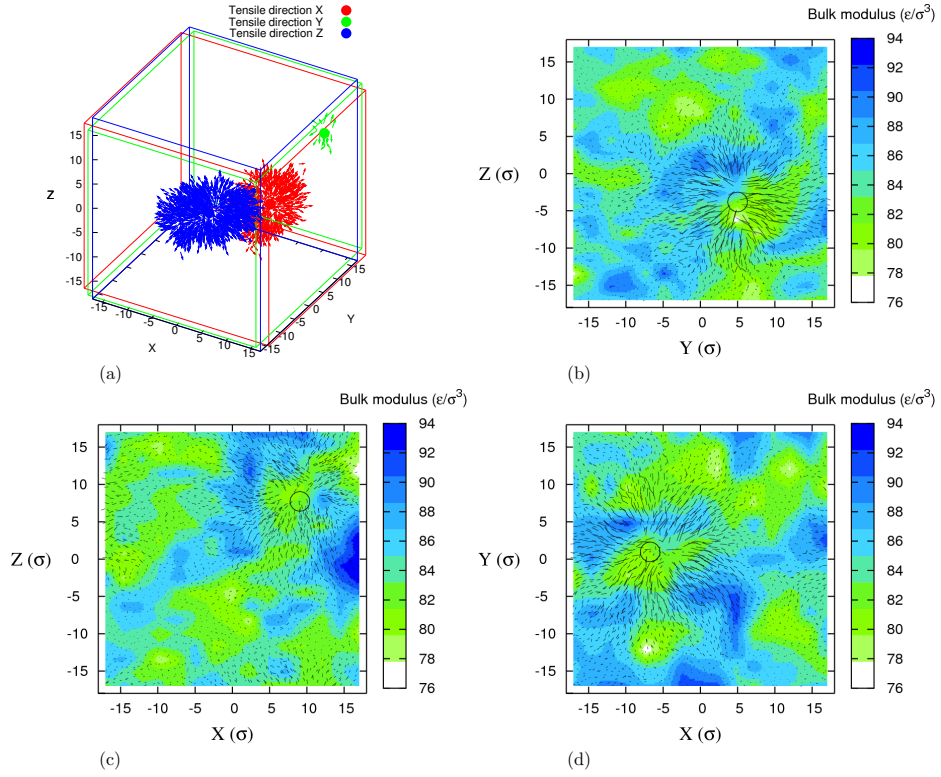


Figure 10: (Color online), (a) Positions of cavities in a single sample after tensile tests with different straining directions. The vectors describing the formation of a cavity are superimposed with the corresponding map of local elastic bulk modulus imaged in the initial, undeformed, configuration. Slices (b), (c) and (d) are located in the corresponding position of the cavity nucleation and they are perpendicular to the tensile directions X, Y and Z, respectively.